Evidence for helical microstructure of aragonite fibers in pteropod shells

Antonio G. Checa,* Carlos Pimentel, Katarzyna Berent, Paula Ramos-Silva, Alejandro B. Rodríguez-Navarro, Julyan H.E. Cartwright, and Claro I. Sainz-Díaz

Planktonic gastropods of the suborder Euthecosomata (order Pteropoda) secrete a unique microstructure made of tightly interlocked, space-filling helically coiled aragonite fibers. This material has a high degree of ordering because all fibers are in phase at a given growth plane. The recognition of the helical nature from mere scanning electron micrographs is somewhat uncertain. In addition, three-dimensional (3D) reconstructions of individual helices are hindered by the small dimensions of fibers, and the virtual absence of intervening organic interphases. Here, we (1) reexamine the morphological characteristics of the fibers in fracture and find them compatible with a helical model, (2) provide direct evidence of the helical mode of coiling in the form of anaglyphs, and (3) develop a 3D model, which is fully consistent with the patterns observed in fractures and polished sections. Proposals based on motifs different from helices are not congruent with the observations.

Impact statement

Some planktonic gastropods of the order Pteropoda secrete a unique microstructure that was originally described as made of tightly interlocked helically coiled continuous aragonite fibers. Despite this material having been described 50 years ago, there is still debate as to the helical design of such fibers. We provide additional unambiguous evidence that fibers describe true helical trajectories during growth. Establishing their true nature is essential in order to know the spectrum of calcified biomaterials produced by molluscs. This is also a prerequisite for future biomimetic studies aiming at producing bioinspired highly functional materials.

Introduction

Out of more than a dozen basic biomineral microstructures secreted by molluscs, the most unusual one is the helical microstructure, composed of helically coiled aragonite fibers. To date, it has only been recognized in pteropods, a group of planktonic gastropods that appeared in the Early Cretaceous.[1] The helical microstructure was first fully described for the species *Cuvierina columnella*.[2] The presence of this microstructure was further confirmed in all the other members of the Cavolinioidea,[3–6] a superfamily with an accepted diversity of 63 species, 10 genera, and 5 families.[7] It was also recognized in the genus *Heliconoides*,[4] a member of the Limacinoidea, the sister group of the Cavolinioidea. Both Cavolinioidea and Limacinoidea compose the suborder Euthecosomata. The helical microstructure is made up of thin fibers (~300 nm wide) of aragonite, which coil dextrally. Each fiber has its own coiling axis, which is slightly displaced with respect to those of its neighbors. All fibers turn around axes parallel to each other and perpendicular to the shell surface and have identical morphologies (radius, lead angle).[2] During growth, all helical trajectories are

in phase, that is, at a given growth increment they display exactly the same orientation. Fibers interlock tightly, which allows them to fill all the available volume. This structure limits mechanical damage by forcing tortuous crack propagation, thus, making these ultrathin shells an effective protection for the living tissues of the animal.[8,9] Details about the cross-sectional shapes of the fibers and their interpenetration patterns have been described by previous authors.[2,5,8] Although interesting, however, these aspects are not relevant for the purpose of the present work.

Based on transmission electron microscopy (TEM) and electron backscatter diffraction (EBSD), Willinger et al.[10] found that each fiber shows crystallographic continuity and is composed of a myriad of aragonite crystals twinned on {110}. The *c*-axis is along the coiling axis, and there is a trend to grow along the projection of the *b*-axis. Conversely, Suzuki et al.[11] proposed that the fibers are composed of segments with slightly divergent orientations. From the evidence they provided, it is unclear that the areas they measured belonged to a single fiber.

What is extraordinary regarding this microstructure, is (1) the helical nature of the fibers, (2) the crystallographic continuity of the fibers, (3) the high degree of similarity and ordering of the helices, and (4) their strict interlocking.

The helical nature of the fibers is not immediately evident in the published images of fractures both because (1) the distribution of the gray hues in SEM depends on the orientation with respect to the detector and is not comparable to natural lighting, and (2) the fibers show limited continuity both in fracture and, especially, in section. In some instances, the continuity of fibers in fractures can be traced from around half a whorl[5,8–12] to one complete whorl.[2,8] Nevertheless, the helical coiling is not immediately evident in the absence of unambiguous information on the depth dimension.

The helical path of the fibers was first shown in detail by Bé et al.,[2] who provided stereoscopic photographic pairs where the helices are clearly discernible, particularly in their plate 4 (Figures 1, 2), plate 9 (Figure 3), and plate 16 (Figures 1, 2). Later, Zhang et al.[8] showed for *Cavolinia uncinata* that the change in aspect of the fiber arrangement in fracture with inclination is consistent with helical coiling. In addition, they showed by progressive layer-by-layer polishing perpendicular to the shell surface that the fibers rotated for about 300 degrees. All other studies assumed the helical nature of fibers and added scanning electron microscopy (SEM) photographs of either fractures[4–6,8–14] or polished sections.[6,8,9,11]

Recently, Sibony-Nevo et al.[15] have proposed an alternative model for the microstructure of the shell of the cavolinioidean *Creseis acicula* based on focused ion beam (FIB)-SEM slice and view, according to which the fibers do not form helices but S-shaped motifs arranged in planes at an angle between 15° and 25° to the outer shell surface. The main problem was that the technique used did not allow these authors to resolve individual fibers.
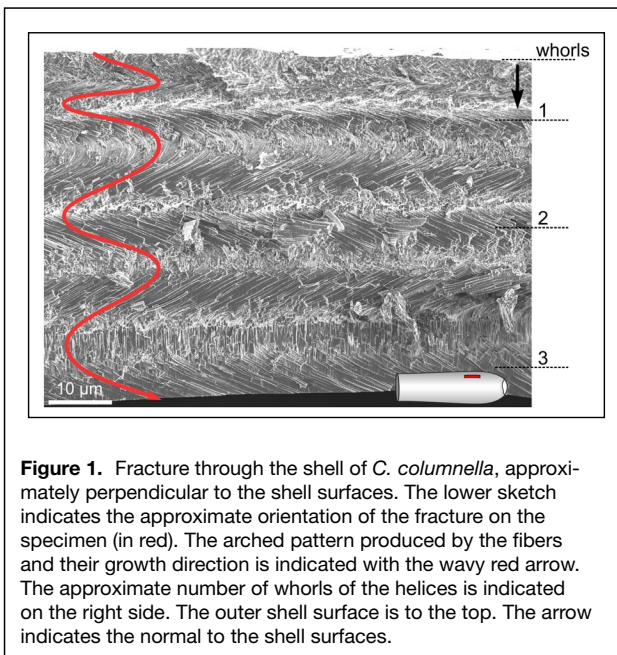

Figure 1. Fracture through the shell of *C. columnella*, approximately perpendicular to the shell surfaces. The lower sketch indicates the approximate orientation of the fracture on the specimen (in red). The arched pattern produced by the fibers and their growth direction is indicated with the wavy red arrow. The approximate number of whorls of the helices is indicated on the right side. The outer shell surface is to the top. The arrow indicates the normal to the shell surfaces.

In order to dispel any uncertainty about the helical nature of the fibers of the cavolinioidean gastropods, we have carried out an SEM-based study of their microstructure. By harnessing the present capabilities of the SEM-associated software to provide 3D effects, we demonstrate that the fibers making up the shells of the cavolinioideans coil helically. In addition, we develop a theoretical model that predicts that a volume filled with evenly sized/shaped helices provides arched patterns when sectioned. The exact shape of the arches (wavelength) depends on how the volume is sectioned.

All in all, we provide novel information, which complements previous evidence and is essential to demonstrate the helical coiling of the fibers of the studied pteropods.

Results and discussion

Most of our observations have been made on fractures approximately perpendicular to the shell surfaces, which is how the material generally breaks by pressing the curved shell surfaces. Such fractures reveal the presence of a series of continuous arches, which propagate from the outer to the inner surface of the shell in the form of a wave with an approximately constant amplitude. In *Cuvierina*, where the number of turns is maximal (slightly more than three), views of the whole cross sections reveal that wavelength increases toward the internal shell surface (**Figure 1**). The FFT patterns of such sections are characteristically six-rayed due to the regular arrangement of fibers and the sinusoidal shape of the helical microstructure when projected in two dimensions (Figure S1 in the Supplementary Material).

Even though there is not a strictly consistent fracturing pattern, the fibers tend to break along their length when they run parallel to the fracture plane and along their thickness as the
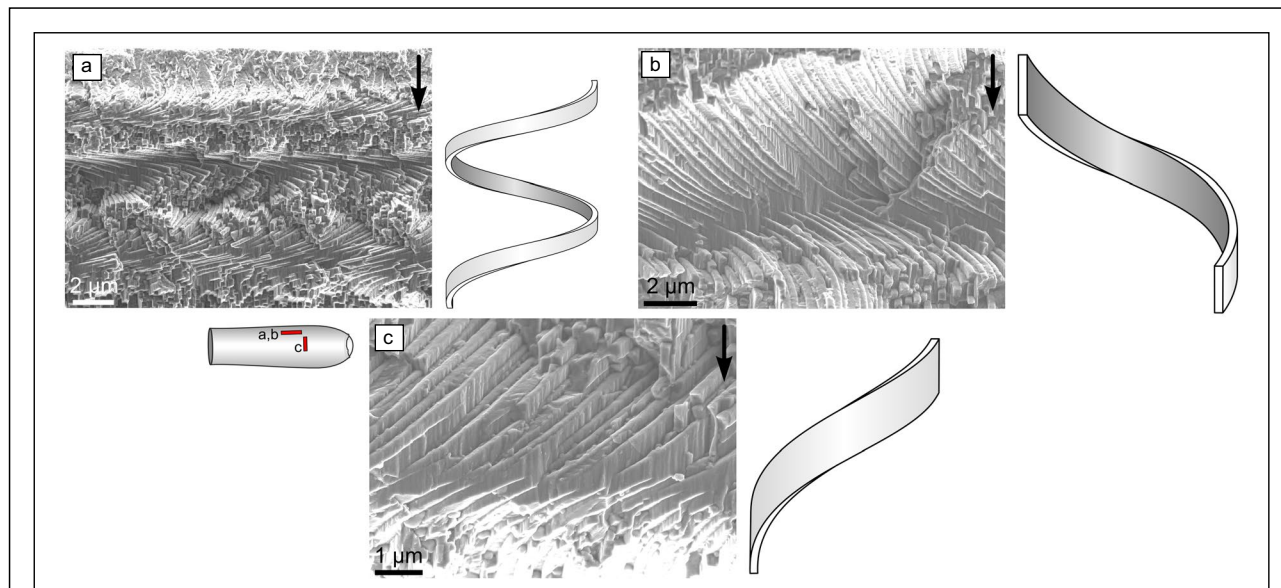
Figure 2. Close-up views of fractures approximately perpendicular to the shell surfaces of *C. columnella* (a–c). The orientations of the fractures are indicated in red in the small sketch of a complete specimen. The areas where the fibers change their direction from toward the background to the foreground appear in low relief (a, b), and where they curve again toward the background they are in high relief (a, c). The sketches indicate the approximate tracing of an ideal fiber. Fibers become displaced with growth around and along the coiling axis toward the inner shell surface (i.e., toward the bottom of the images). The arrows indicate the normals to the shell surfaces.
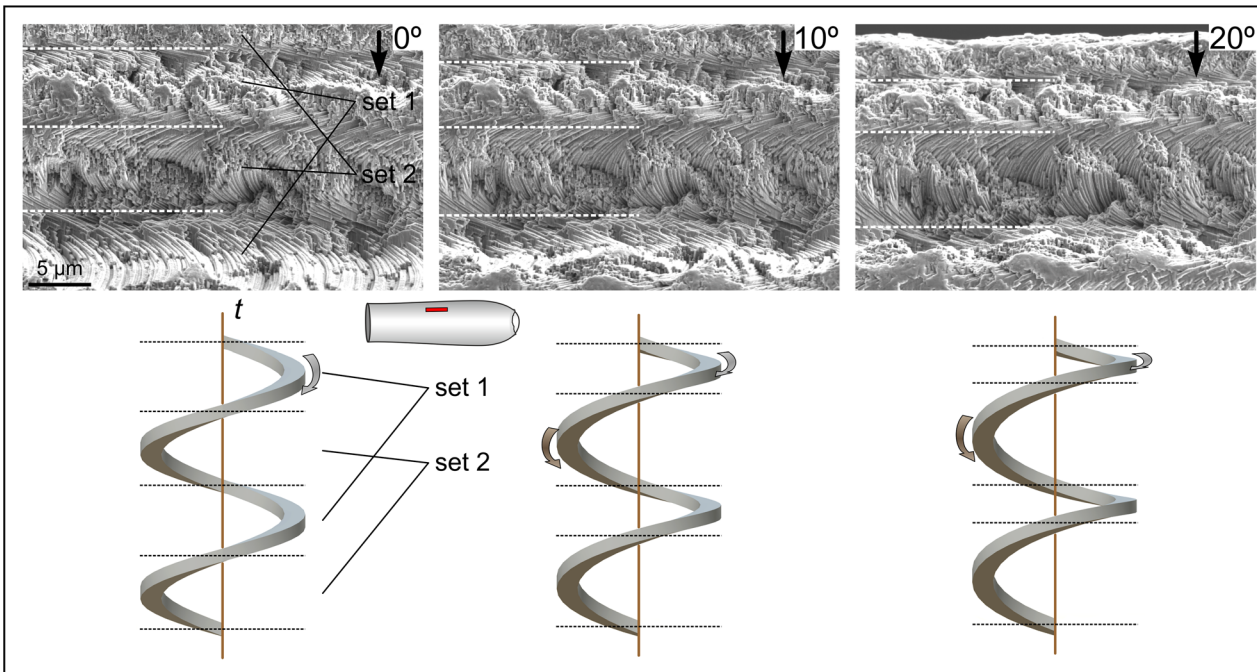

Figure 3. Changes in the relative dimensions of the half turns with tilting of the coiling axes of the helices. The upper row is a series of images of the same area of a fracture of *C. columnella* at different inclination angles (indicated). The orientation of the fracture is indicated in red in the small sketch of a complete specimen. With growth, all fibers translate toward the inner shell surface (located toward the bottom of the images). Half whorls are distinguished with broken lines traced at the positions where the helices run parallel to the image. Note the increasing difference of the apparent distance between half whorls of sets 1 (those growing toward the foreground) and 2 (those growing toward the background) with increasing inclination angle of the top end of the coiling axis (located at the top of the images) toward the background. The arrows on the SEM images indicate the normals to the shell surfaces. The lower sketches replicate the process with theoretical helices (*t* is the top end of the coiling axis). The arrows indicate the growth directions of the half whorls.

fibers become perpendicular to the fracture plane (**Figure 2**). Upon fracturing, when the half whorls change their growth directions from toward the background to the foreground, they tend to show in low relief (Figure 2a–b), whereas those changing from toward the foreground to the background tend to stand out in high relief (Figure 2a, c). Fibers most often break where they are at a high angle to the plane of viewing (Figure 2a–b). Accordingly, the best areas for observation of fiber continuity are where the fibers are approximately parallel to the fracture plane (Figure 2). Although continuity of single fibers can rarely be traced for more than half a turn, they can be followed for longer by correlating different areas (e.g., Figure 2a).

Due to the described fracturing pattern, when the fracture surfaces are inclined with respect to the observation plane (e.g., because the fragment is not vertical on the SEM stub and is tilted toward one of the shell surfaces), there is a set of half whorls (those growing opposite to the tilting direction; set 1) that is seen more and more in profile, whereas the set growing toward the tilting direction (set 2) becomes more and more exposed in plan view. An example taken from *C. columnella* is provided in **Figure 3** (top row), together with a series of explanatory sketches (Figure 3, bottom row). As the top end of the coiling axis (to the top of the images) becomes progressively tilted toward the background, the apparent dimensions of the half whorls of set 1 diminish, even to the point of concealment, whereas the reverse is true for the half whorls of set 2. This observation is consistent with the helical nature of the fibers. A similar test was presented earlier on *C. uncinata*,[8] although with much higher tilting angles.

Definite evidence of the helical nature of the fibers is provided here by 3D images in the form of anaglyphs. Several examples of anaglyphs together with the corresponding sketches depicting the idealized coiling pattern, from *C. columnella*, *C. pyramidata*, *D. trispinosa*, *C. inflexa*, and *C. acicula* are provided in **Figure 4**. They show without any doubt that the fibers coil helically, even if for small amounts of rotation (e.g., Figure 4b). The only exception is *C. acicula*, which shows a helical pattern close to the apical area (Figure 4g), whereas more toward the aperture fibers display a short external helical part, a middle very open S-shaped part and an internal helical part (Figure 4h and S2 in the Supplementary Material). The different stages are short and the fibers coil for less than half a whorl in either of the external and internal helical stages. For regularly coiled fibers, we provide evidence of coiling for up to 2.5 whorls in *Cuvierina* (Figure 4a). By comparing (e.g., Figure 1 with Figure 4a), it becomes clear that each pair of contiguous arches looking in opposite directions in normal SEM images corresponds to one complete turn.

Our 3D theoretical model is provided as a helical model in the Supplementary Material. It is an html file, which can be run in any browser. It shows that when we section a volume containing in-phase helically coiled fibers (as in the shells of cavolinioideans) parallel to the coiling axis, a pattern in the

form of arches in both directions arises, composing a wavy pattern. The waves are not made of single fibers but by juxtaposed sections of fibers. These appear more and more elongated as they become farther away from the crests/troughs of the wavy pattern (**Figure 5**a, frontal section). Given the rotational symmetry of the helical coiling, any sectioning plane containing the coiling axis would always produce this same pattern (compare frontal, lateral views, and the section at 45 degrees in Figure 5a). This is consistent with the patterns observed in shell fractures (Figures 1 and 4) and is identical to those obtained on polished/etched sections (Figure 5b; see additional examples in References 6, 8, 9, and 11). When the sectioning plane is at an angle to the coiling axis, the arched pattern is qualitatively the same, although the wavelength of the arches increases with the deviation angle (Figure 5a, sections at 30 and 60 degrees). Only when the sectioning plane is perpendicular to the coiling axes of fibers (top view), the pattern ceases to be wavy (Figure 5a).

Sibony-Nevo et al.[15] derived their planar S-shaped fiber hypothesis from sections inclined between 15 and 25 degrees to the outer shell surface, obtained with the FIB-SEM *slice and view* technique. They interpreted the resulting S-shaped fiber arrangement (consistent with obliquely sectioned helical fibers; see above) as corresponding to the actual fiber shape. It is to be stressed that the technique employed did not allow them to resolve individual fibers. A theoretical model based on a series of inclined nested S-shaped fibers arranged in planes (Figure S3 in the Supplementary Material, and sigmoidal model in the Supplementary Material) shows that in sections perpendicular to the shell surfaces, the patterns change depending on whether the vertical cut is transversal or parallel to the propagation direction of the fibers. In the first case, we only see a surface tiled with similarly shaped transversal sections of the fibers. In the section parallel to the propagation of the fibers, the tiling consists of more (when the section goes through the crests/troughs of the sigmoids) or less (flanks) elongated straight sections. A sigmoidal pattern would only be obtained in a section parallel to the fiber axes. The horizontal cut provided in Figure S3 in the Supplementary Material shows a quasi-sigmoidal pattern consisting of similarly elongated fiber sections. Sibony-Nevo et al.'s[15] data came from the species *C. acicula*, which we also examined here. The microstructure is helical close to the apical end, as in the rest of the cavolinioideans (Figure 4g). In all specimens examined, more toward the aperture, the fibers unwind and follow a transitory S-shaped path in the central part of the shell wall (Figures 4h and S2 in the Supplementary Material). This is a transitory pattern that is lost as the shell thickens. As shown in our theoretical helical and sigmoidal models, it is impossible to distinguish helical from conveniently oriented sigmoidal fibers in section. Accordingly, we cannot know which precise pattern was examined by Sibony-Nevo et al.[15]

In summary, our study provides direct (visual: anaglyphs) and indirect (3D modelization) evidence on the helical coiling of the aragonitic fibers, initially noted by Bé
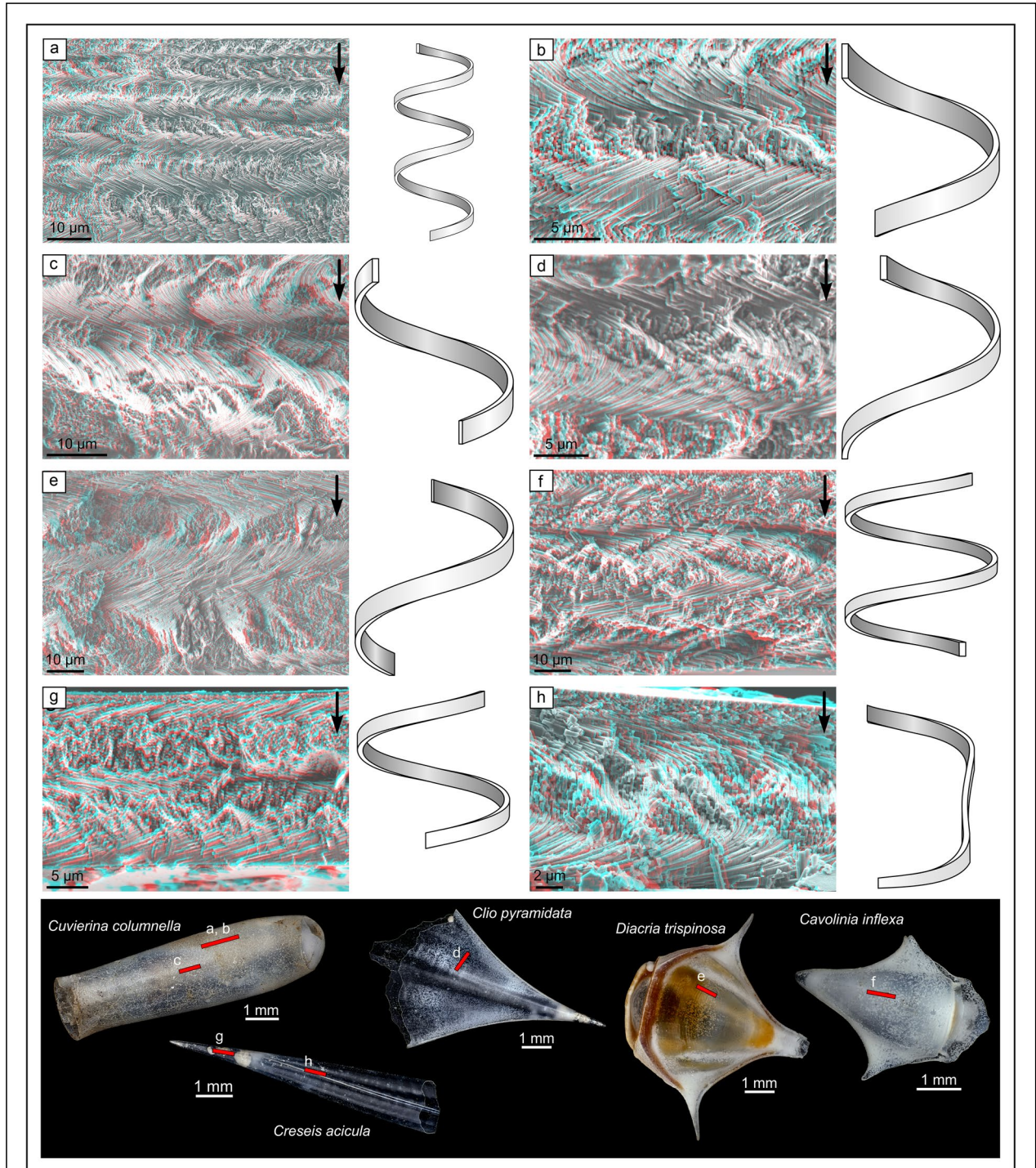
Figure 4. Anaglyphs and sketches depicting the structural motif of fractures approximately perpendicular to the shell surfaces. (a–c) *C. columnella*, (d) *C. pyramidata*, (e) *D. trispinosa*, (f) *C. inflexa*, (g, h) *C. acicula*. (h) A case of nonregularly coiled fibers. Each helical fiber has its own coiling axis. All coiling axes are vertical and parallel to one another in the different images. Growth of fibers proceeds from top to bottom in all cases (i.e., toward the inner shell surface). To appreciate the 3D effect, the anaglyphs have to be observed with red/cyan glasses. The arrows indicate the normals to the shell surfaces. The orientations of the fractures are indicated (red rectangles) on selected specimens of the mentioned species (bottom part of the figure).
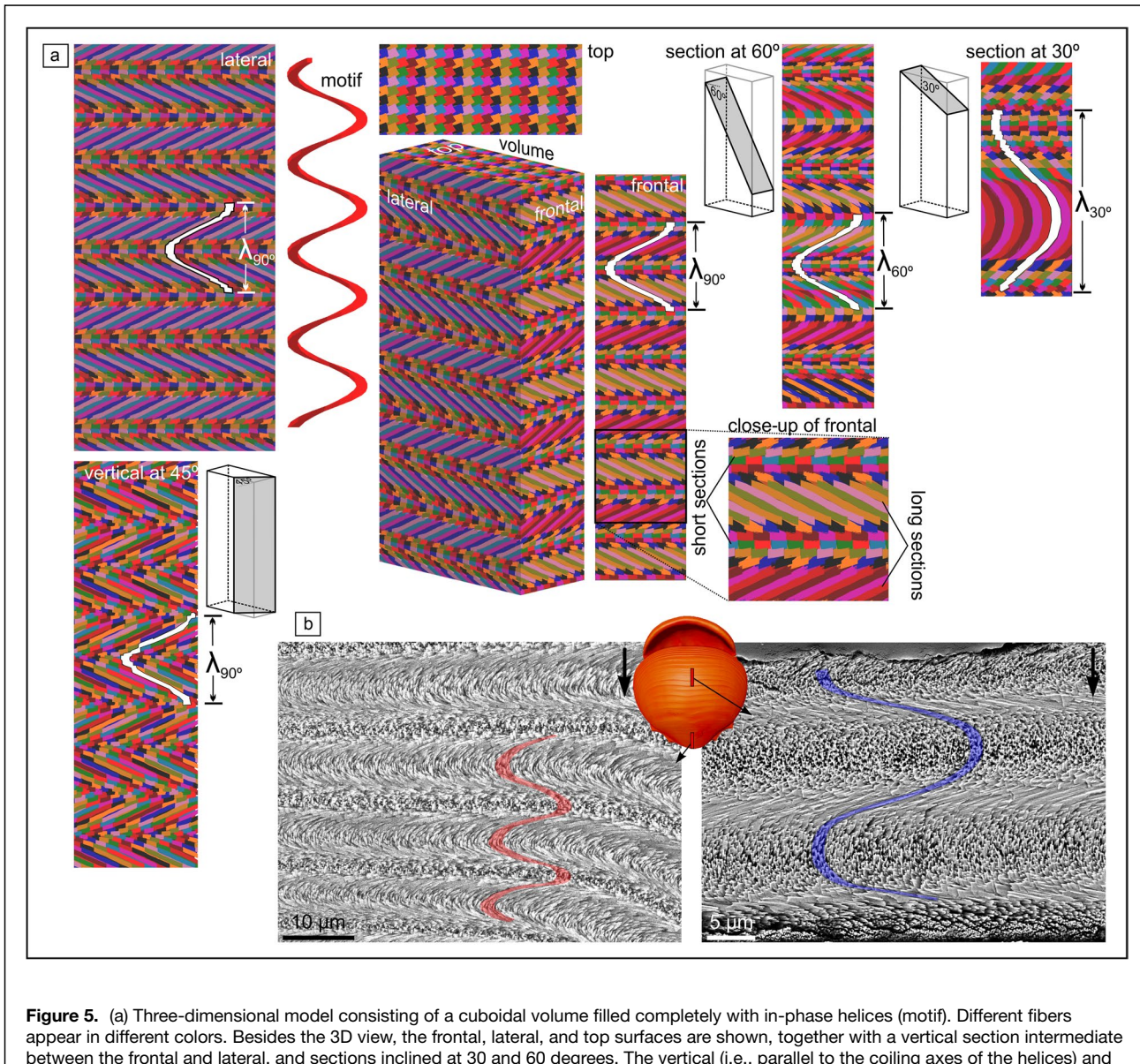
Figure 5. (a) Three-dimensional model consisting of a cuboidal volume filled completely with in-phase helices (motif). Different fibers appear in different colors. Besides the 3D view, the frontal, lateral, and top surfaces are shown, together with a vertical section intermediate between the frontal and lateral, and sections inclined at 30 and 60 degrees. The vertical (i.e., parallel to the coiling axes of the helices) and oblique sections display arched patterns constituted by elongate sections (at the flanks of the sinusoids), followed by short transversal section at the crests, as can be seen in the close-up view of the frontal side of the cuboid. A wave has been outlined (in white) for a complete wavelength on each section. As the inclination of the sectioning plane becomes higher, the wavelength becomes smaller (following the sequence $\lambda_{30°} > \lambda_{60°} > \lambda_{90°}$). The wavelength is identical for all vertical sections. The wavy pattern is absent in the horizontal (top) section, which only provides homogeneously shaped, sized, and oriented fiber sections. (b) Two images of polished/etched sections perpendicular to the shell surfaces of *Diacria costata*, showing the resulting arched pattern (outlined in color). The position of the sections on the shell is indicated (in red) on a micro-CT image of a specimen. The arrows indicate the normals to the shell surfaces. Note the coincidence with the vertical sections in the theoretical model. Fibers grow toward the inner shell surface (located toward the bottom of the images).

et al.[2] Our and previous complementary evidence[2,8] leaves little room for doubt on this issue. Future 3D reconstructions of the actual fibers (not attainable today) may provide additional information on their growth dynamics (coiling parameters, interlocking, division…). In this way, we hope to add significantly to the "Wavy or curly?" debate proposed by Gilbert.[16]

Material and methods

Material

We examined material of the cavolinioideans *C. columnella* (Cuvierinidae) (twelve specimens), *C. pyramidata* (Cliidae) (three specimens), *C. acicula* (Creseidae) (five specimens), *C. inflexa* (three specimens), *D. trispinosa* (four specimens), and *D. costata* (Cavolinidae) (two specimens). Specimens of the

five first species came from the Banc Atlantis, N–O "le Suroit" Seamount 2, Atlantic Ocean, 34°22, 4′ N, 30°27, 80′ W, dredged from 1340 m, and were acquired on loan from the Muséum National d'Histoire Naturelle, Paris (France). Specimens from *D. costata* came from the North Pacific, Hawaii (22°34.4 N, 157°40.8 W; Cruise ID KOK1703) and are deposited in the Naturalis Biodiversity Center (Leiden, The Netherlands).

Scanning electron microscopy

Specimens of all species, except for *D. costata*, were fractured by pressing the shells between two glass plates. Given the vaulted morphology of the shells, the fractures tended to be perpendicular to the shell surfaces. Some samples were cleaned by immersing them in commercial bleach (4% active chlorine) for 1–4 min and subsequently ultrasonicated in Milli-Q water. The fragments were placed on an SEM stub coated with adhesive carbon tape, such that the shell wall was approximately perpendicular to the stub surface. Samples were coated with carbon in a Hitachi UHS evaporator, prior to examination in either of the two FESEMs (FEI Qemscan 650F, and Zeiss Auriga Cross-Beam Station), at the Centro de Instrumentación Científica (CIC) of the Universidad de Granada (UGR), Spain. Other specimens were carbon coated with a Quorum Technologies Q150T E sputter coater and examined in the FEI Versa 3D FESEM at the Academic Centre for Materials and Nanotechnology, ACMiN, AGH University of Science and Technology (UST), Kraków, Poland. The fast Fourier transform (FFT) of some images was calculated by using the FFT tool of the ImageJ software (version 1.53 k, National Institutes of Health, USA). The brightness and contrast were adjusted automatically using the same software.

Shells of *D. costata* were embedded in LR White Medium resin (London Resin). Cross sections of the solid resin were prepared using a cross-sectioning Leica sp1600 saw microtome. Mirror polishing of the cross sections was made using a Minitech 233 with grinding disks of P320, P600, P1200, P4000, and 0.05 μm aluminum oxide paste. Polished surfaces were etched with EDTA 1% for 1 min, rinsed with distilled water, and dried. All samples were sputter coated with gold using a DII-29030SCTR (Smart Coater) and observed with a FESEM JEOL JSM-IT100LA at an acceleration voltage of 15 kV at the Laboratoire Biogéosciences UMR CNRS 6282 of the University of Burgundy-Franche-Comté (Dijon, France), or with a JEOL JSM-7600F under an acceleration voltage of 5 kV at Naturalis Biodiversity Center (Leiden, The Netherlands).

Three-dimensional images (anaglyphs)

Anaglyphs are stereoscopic images that are created by overlapping two SEM micrographs recorded for different perspectives, thus forming a stereoscopic pair. By merging both images, a 3D effect of the imaged area is obtained. SEM micrographs of investigated samples were obtained in both the FEI Quanta 400 (CIC, UGR) and the FEI Versa 3D (ACMiN, AGH UST) FESEMs. Imaging was performed in high vacuum mode using a secondary electron detector at an acceleration voltage of 5 kV. In a first step, the SEM micrograph was acquired at a tilt angle of 0° and a working distance (WD) of 10 mm. An eucentric point was used, which enabled pure tilting without introducing any lateral translation. Then, the specimen was tilted along a vertical axis (i.e., perpendicular to the axis joining both eyes of the observer) at 5° and/or 8°, and a second SEM image was recorded at the same magnification and WD.[17,18] Both SEM images were later merged and read into the xT microscope Control software (FEI, Hillsboro, OR, USA), turned into red and cyan images, and then overlapped using the "stereo pair" option. Figures 4 and S2 in the Supplementary Material show the red-cyan anaglyphs of different cavolinioidean species with sufficient parallax effects. The 3D effect is fully appreciated by observing them with easily obtainable red/cyan glasses.

Three-dimensional theoretical models

The design of the 3D models of the helices and sigmoids was carried out using FreeCAD software.[19] The helical model (helical model in the Supplementary Material) was designed in the part workbench using the helix tool inside the primitives menu. The radius of the helix was set at 10 mm and the pitch at 30 mm. The height of the helix was set at 150 mm. Once the helix was built, the next step was to give it volume. For this, we used the design part workbench. In this section, we used the sketch tool. The *XZ* plane was established as the work plane and a rectangle of 3 × 1.5 mm was drawn. At last, the rectangle was used as the profile and the helix as the trajectory. The options solid and frenet were also checked. This was done in the part workbench with the sweep tool.

The sigmoid model (sigmoidal model in the Supplementary Material) was designed in the part design workbench too. First, the sigmoid was designed by setting up the *XY* plane as working plane using the sketch tool. On this plane, the sigmoid was drawn using the B-spline tool. The next step was to draw a rectangle in the *XZ* plane and to make a sweep, as previously explained. Once the initial helix and sigmoid models were designed, they were replicated in order to obtain a volume. The cuboid was designed by cutting the volume with orthogonal planes. This also enabled the visualization of the intersections between these planes and the designed 3D models. The last step was to export these models from the original .FCStd file to the definitive .html files included in the Supplementary Material. The .html files can be viewed in any web browser.

Data availability

All the data are available from either A.C.G., K.B., P.R.-S. (SEM images, and their anaglyphs and 3D views) or C.P. (theoretical models).

Code availability

Software: ImageJ Version 1.53 k RRID:SCR_003070.

Conflict of interest

The authors have no competing interests to declare.

Ethical approval

Not applicable.

Consent to participate

Not applicable.

Consent for publication

Not applicable.

Supplementary information

The online version contains supplementary material available at https://doi.org/10.1557/s43577-022-00418-y.

References

1. K.T.C.A. Peijnenburg, A.W. Janssen, D. Wall-Palmer, E. Goetze, A.E. Maas, J.A. Todd, F. Marlétaz, *Proc. Natl. Acad. Sci. U.S.A.* **117**, 25609 (2020). https://doi.org/10.1073/pnas.1920918117
2. A.W.H. Bé, C. MacClintock, D.C. Currie, *Biominer. Res. Rep.* **4**, 47 (1972)
3. J. Rampal, "Les Thecosomes: Systématique et Évolution, Écologie et Biogéographie Méditerranéennes" PhD thesis, L'Université de Provence Aix, Marseille I. (1975), p. 485
4. G. Glaçon, J. Rampal, D. Gaspard, D. Guillaumin, T.S. Staerker, *Proc. Ocean Drill. Progr.* **134**, 319 (1994). https://doi.org/10.2973/odp.proc.sr.134.014.1994
5. A.G. Checa, E. Macías-Sánchez, J. Ramírez-Rico, *Sci. Rep.* **6**, 25989 (2016). https://doi.org/10.1038/srep25989
6. P. Ramos-Silva, D. Wall-Palmer, F. Marlétaz, F. Marin, K.T.C.A. Peijnenburg, *J. Struct. Biol.* **213**, 107779 (2021). https://doi.org/10.1016/j.jsb.2021.107779
7. WoRMS Editorial Board, *World Register of Marine Species* (2021). http://www.marinespecies.org at VLIZ. Accessed 2 Dec 2021
8. T. Zhang, Y. Ma, K. Chen, M. Kunz, N. Tamura, M. Qiang, J. Xu, L. Qi, *Angew. Chem. Int. Ed.* **50**, 10361 (2011). https://doi.org/10.1002/anie.201103407
9. L. Li, J.C. Weaver, C. Ortiz, *Nat. Commun.* **6**, 6216 (2015). https://doi.org/10.1038/ncomms7216
10. M.G. Willinger, A.G. Checa, J.T. Bonarski, M. Faryna, K. Berent, *Adv. Funct. Mater.* **26**, 553 (2016). https://doi.org/10.1002/adfm.201504034
11. M. Suzuki, T. Sasaki, Y. Oaki, H. Imai, *Cryst. Growth Des.* **17**, 191 (2017). https://doi.org/10.1021/acs.cgd.6b01417
12. D. Curry, J. Rampal, *Malacologia* **18**, 23 (1979)
13. L.M. Roger, A.J. Richardson, A.D. McKinnon, B. Knott, R. Matear, C. Scadding, *ICES J. Mar. Sci.* **69**, 465 (2012). https://doi.org/10.1093/icesjms/fsr171
14. H.H. Baron, "Characterization of Shell Microstructures and the Shell-Tissue Interface of Shelled Pteropods from Cavoliniidae Family," MSc thesis, Weizmann Institute of Science, Rehovot (2014), p. 40
15. O. Sibony-Nevo, K. Rechav, V. Farstey, E. Shimoni, N. Varsano, L. Addadi, S. Weiner, *MRS Bull.* **47**(1), 18 (2022). https://doi.org/10.1557/s43577-021-00184-3
16. P.U.P.A. Gilbert, *MRS Bull.* **47**(1), 16 (2022). https://doi.org/10.1557/s43577-021-00229-7
17. R. Sturm, *Micros. Today* **26**, 34 (2018). https://doi.org/10.1017/S1551929518000640
18. J. Xie, Stereomicroscopy: 3D Imaging and the Third Dimension Measurement (Agilent Technologies Application Note, 2011). http://www.toyo.co.jp/files/user/img/product/microscopy/pdf/5990-9127EN.pdf
19. J. Riegel, W. Mayer, Y. Van Havre, FreeCAD 0.19 (2021). https://www.freecadweb.org/ □